Organic & Biomolecular Chemistry

Accepted Manuscript

ROYAL SOCIETY OF CHEMISTRY

www.rsc.org/obc

Journal Name

RSCPublishing

ARTICLE

Monitoring and Inhibition of Plk1: Amphiphilic porphyrin conjugated Plk1 specific peptides for its imaging and anti-tumor function

Cite this: DOI: 10.1039/xoxxoooooox

Received ooth January 2014,
Accepted ooth January 2014

DOI: 10.1039/xoxxoooooox

www.rsc.org/

Hongguang Li,[a] Chi-Fai Chan,[a] Wai-Lun Chan,[a] Sam Lear,[b] Steven L. Cobb,[b*] Nai-Ki Mak,[c] Terrence Chi-Kong Lau,[d] Rongfeng Lan,[e*] Wai-Kwok Wong,[a*] and Ka-Leung Wong[a*]

Polo-like kinase 1 (Plk1) is well-known for taking part in cell cycle progression and regulation. Using small molecules for Plk inhibition has been well documented in the literature. However, there are several intrinsic and intractable problems associated with this approach. For example monitoring small molecule Plk inhibitors as anti-tumor agents *in vitro/in vivo* is often ineffective, they can have poor cell internalization and be susceptibility to enzymatic degradation. Herein, we report the synthesis of a cell-permeable, water-soluble amphiphilic porphyrin – Plk1 specific peptide bioconjugates, Por-1 and Por-**P2**. In addition to resolving the aforementioned problems of the small molecule inhibitors Por-**P2** manifests responsive emission enhancement upon binding with Plk1 in aqueous and *in vitro*, while potently triggering G2-M phase arrest and then apoptosis selectively in the cancer cells tested. In combination our findings make Por-**P2** a promising candidate for the preparation of a a new generation of smart chemotherapeutic targeting agents (imaging and inhibition) for Plk1 in particular cancer cell lines.

Introduction

Polo-like kinase 1 (Plk1) is a critical cyclin-independent serine/threonine protein kinase involving in many central cell cycle events. Within the molecule, Plk1 offers two distinct drug (anti-cancer) targets: an N-terminal catalytic domain and a C-terminal polo-box domain (PBD) that are responsible for the recognition of phosphorylation sequence and binding of the substrates.[1] Unlike normal cells, cancer cells have a higher demand for polo-like kinases to maintain cell cycle activities; hence some studies have found that the loss of Plk1 expression inside tumors can induce pro-apoptotic pathways and growth inhibition.[2] To date, a few small molecules, such as ATP analogues and Plk-specific peptides, have been developed to inhibit Plk1 for cancer therapy. However, it is ineffectual for the former to bind to the kinase domain rather than the PBD and to be visualized indirectly, with their activation details/binding dynamics being uncertain as well.[3-11] The latter, even if it is able to block the PBD and potentially kill tumor cells via binding and inhibiting the highly expressed Plk1, suffers significantly from the poor cellular uptake efficiency.[12] In this regard, a specific dual-function agent capable of simultaneous optical imaging and inhibition can help scientists to study Plk1 more comprehensively and conveniently at both cellular and molecular levels.

Herein, two water-soluble porphyrin-based compounds (Por-**P1** and Por-**P2**) had been synthesized with two different Plk1 specific peptides (**P1** and **P2**) (Fig. 1 and S1, ESI†). Comprehensive studies of their structural designs and *in vitro* activities had been carried out with various experimental methods. It is the amphiphilic nature of our designed compounds that (hydrophobic-porphyrin and hydrophilic-peptides) improves their cell permeability. The binding affinity (via emission and western blot), cellular uptake (via flow cytometry) and selectivity (via selectivity assays against human serum albumin (HSA), bovine serum albumin (BSA), Cyclin A, Cyclin D, bicarbonate and citrate) of Por-**P1** and Por-**P2** had also been carefully examined. Upon administration of Por-**P2**, interruption of the cancer cell growth was observed and direct imaging was possible. Overall, Por-**P2**, exhibited a much stronger enhanced responsive luminescence (detection limit, 2 nM) and much higher cellular uptake and binding affinity for Plk1.Given these factors Por-2 lends itself to being an outstanding dual bio-probe which can be used to both monitor and inhibit Plk1 functions. It is envisaged that the dual action of Por-2 opens up the opportunity to prepare a new-generation anti-cancer agents. Specifically, the combined application Plk1 specific imaging agents and inhibitory small molecules.

Results and discussion

We had estimated the binding fitting via molecular modeling (AutoDock Vina) by comparing interactions between peptides and their porphyrin-peptide conjugates Por-**P1** and Por-**P2**, and the Plk1

protein structure (Fig. S10, ESI†).[13] Peptide **P1** (PLHSpT, the phosphorylated-peptide) and **P2** (PLHSD, the phospho-mimic peptide) had been precisely docked onto the amphiphilic pockets of PBD domain named PB1 and PB2 respectively. The phosphorylated-threonine (pT) or Asp (D) interacts electrostatically with His538 and Lys540, while PLHS formed hydrogen bonding with Trp414 and

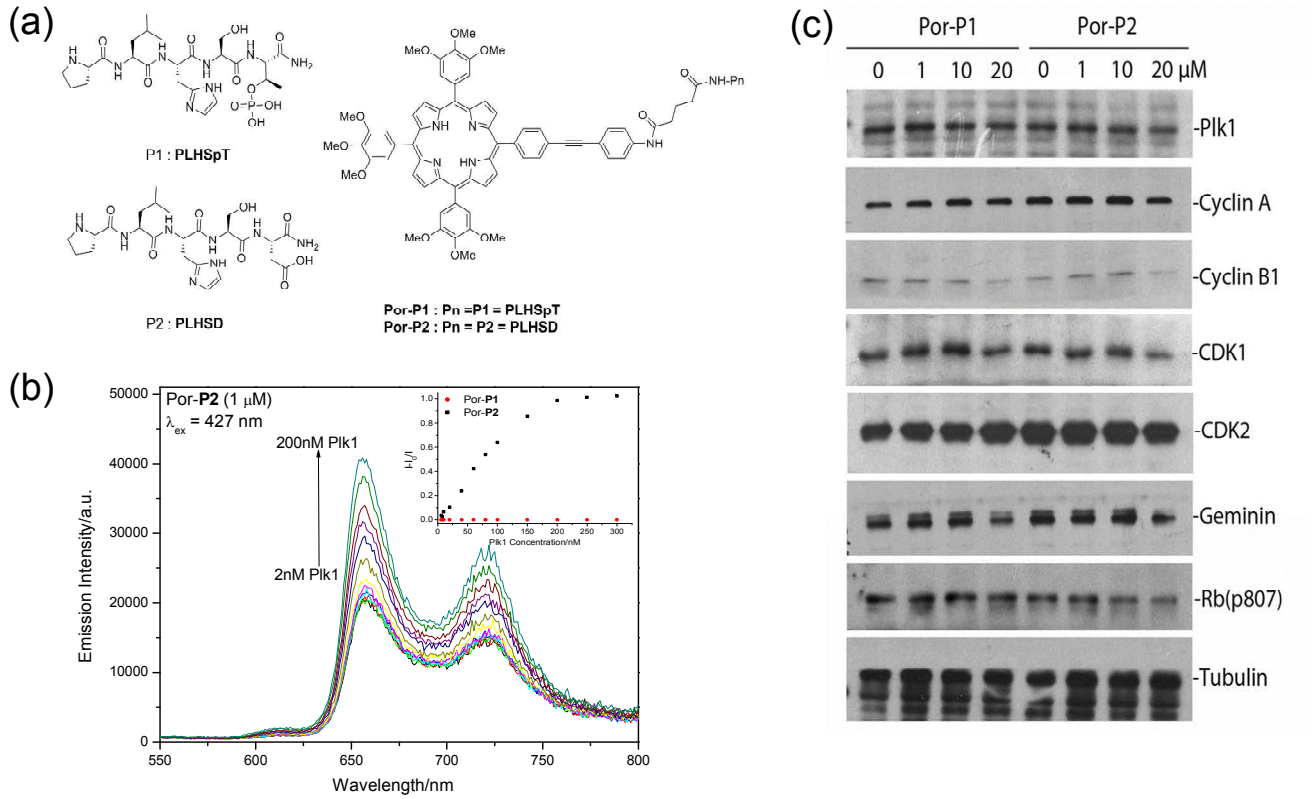

Fig. 1 (a) Chemical structures of the Plk1 specific peptides (**P1** and **P2**), (b) the responsive emission of **Por-P1** upon addition of Plk1 in HEPES buffer, (inset) The plot of the change of porphyrin emission intensity at 650 nm vs. the increasing concentration of Plk1 and (c) Western blotting of key cell cycle regulators in HeLa cells after treated with Por-**P1** and Por-**P2**. Tubulin was blotted as loading control.

van der Waals interactions with β–sheet backone (Phe535). Peptides **P1** and **P2** have theoretical binding energies of -8.1 and -8.2 kCal/mol respectively towards Plk1.

In effect, porphyin-peptide conjugates Por-**P1** or Por-**P2** can provide much diverse and spread binding surfaces to Plk1 due to their extended molecular length and torsions after conjunction with amphiphilic porphyrin. These enhance the binding affinities of Por-**P1** and Por-**P2** to Plk1, with respective calculated values of -8.6 and -9.4 kCal/mol, thereby showing that Por-**P2** does interact more favourably than Por-**P1** with Plk1.

In aqueous solution, Por-**P1** and Por-**P2** give impressive red emissions at ~650 and ~725 nm arising from the porphyrin moiety upon excitation at 430 (linear) or 860 nm (two-photon). The two compounds exhibit similar photophysical properties (emission quantum yield, ϕ_{em} = 22%; singlet oxygen yield, ϕ_{Δ} = 45%; and two photon absorption cross section measured at 860 nm, σ^2 = ~220 GM) Because of the different end group of **P1** and **P2** (**P1** = phosphoric acid and **P2** = carboxylic acid), the pKa values of Por-**P1** and Por-**P2**, are 6.3 and 5.9 respectively. Molecular docking has proposed that two compounds can bind Plk1 well; however, only Por-**P2** can displays an enhancement of the emission upon binding with Plk1. The emission intensity of Por-**P2** was more than double upon addition of Plk1 from 2 nM to 200 nM (Fig. 1b). The selectivity of Por-**P1** and Por-**P2** has been confirmed also by the emission titration in the presence of other biological small molecules and proteins (Fig. S15-S16, ESI†).

As far as the specific impact of our peptide conjugates towards the cellular polo-like kinase is concerned, western blotting was carried out to examine the cells treated with the two candidates (Por-**P1** and Por-**P2**). HeLa cells treated with Por-**Pn** were subject to western blotted against Plk1 as well as key cell cycle regulators Geminin, Rb(p-807), cyclin A or cyclin B1 and their partner kinases CDK1 and CDK2. Cyclin A, cyclin B1 and CDK1 or CDK2 were slightly elevated after the Por-**Pn** treatment, substantiating G2 arrest of cell cycle in 1 and 10 μM, but obviously reduced in 20 μM, which, in turn, suggests the cell death and removal of proteins under severe PlK1 inhibition. These results suggest that Por-**P2** interacted with the polo-like kinase protein in live cells, and that Por-**P1** demonstrated obviously less ability to exert the effect. Experimental results correspond well with the computational one, confirming that Por-**P2** has strong and specific effects on polo-like kinase (Fig. 1c).

Por-**P1** and Por-**P2** have manifested the same detectable emission within the biological window (600 to 800 nm) via linear and near-infrared two-photon excitations at 430 nm and 860 nm respectively. The *in vitro* uptake behaviors of Por-**P1** and Por-**P2** are similar and have been monitored by confocal microscopy in HeLa cells under the same experimental conditions (Fig. 2). From the *in vitro* imaging, the red emission of Por-**P1** and Por-**P2** are observed inside the

cytoplasm in HeLa cells after one-hour incubation. Por-**P1** and Por-**P2** show the red emission *in vitro* with similar subcellular localization, but with different *in vitro* emission intensity. The doubts about the selectivity towards the Plk1 of the two amphiphilic

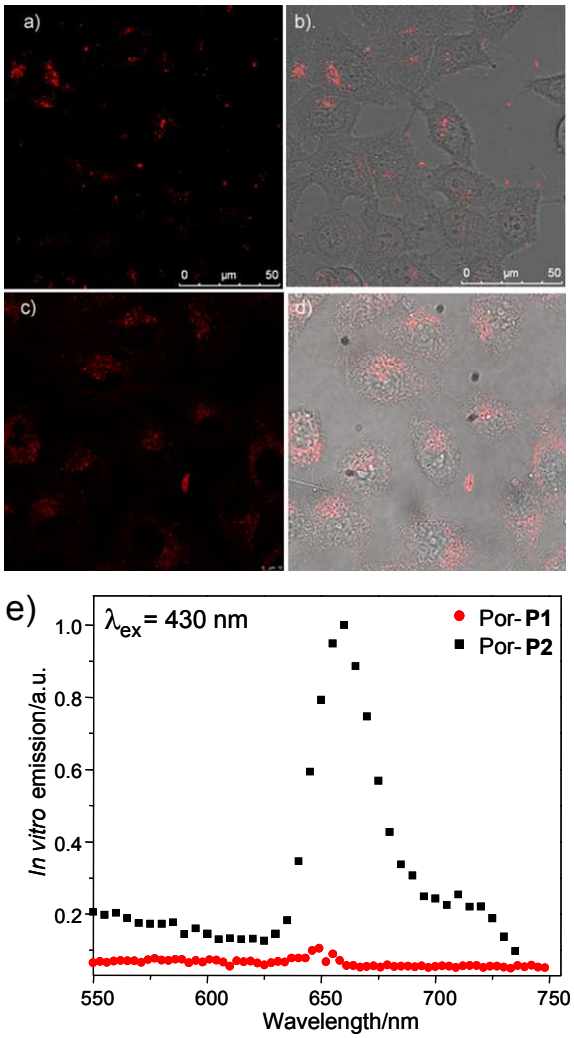

Fig. 2 The two-photon induced (a-d, λ_{ex} = 860 nm) *in vitro* images and linear induced (e, λ_{ex} = 430 nm) *in vitro* emission spectra of Por-**P1** (a and b) and Por-**P2** (c and d) in HeLa cells. (Dosed concentration = 1 μM)

compounds had been overcome with *in vitro* emission spectra in Fig. 2e via lambda scan in confocal microscope (λ_{ex} = 430 nm). The lambda scan inside confocal microscope can be used to monitor the i*n vitro* emission spectra (resolution = 6 nm). Similar to the results of the titration experiments with Plk1 in aqueous solution, the *in vitro* emission intensity of Por-**P2** is much stronger than Por-**P1** under the same excitation and laser power in the HeLa cells (Fig. 2e). The responsive emission *in vitro* indicates the selectivity of Por-**P2** bind toward Plk1 as well.

Overexpressed Plk1 level is well-observed in various kinds of cancer. It is therefore necessary to clarify the inhibitory activity of the two porphyrin moieties (Por-**P1** and Por-**P2**) in cancer (HeLa) and normal (MRC-5) cell lines prior to any further investigation and application. Two experiments (cell cycle flow cytometry, and dark/light cytotoxicity assays) had been carried out to study the capability of Por-**P1** and Por-**P2** to interrupt the cell division. The flow cytometric analysis was conducted to examine the cell cycle phase distribution (G1, G2 and S phases) of the Por-**P1**/Por-**P2** treated HeLa and MRC-5 cells. Treatments with Por-**P1**/Por-**P2** (1 to 20 μmol) and blank (no dosage of compounds) had been worked out.

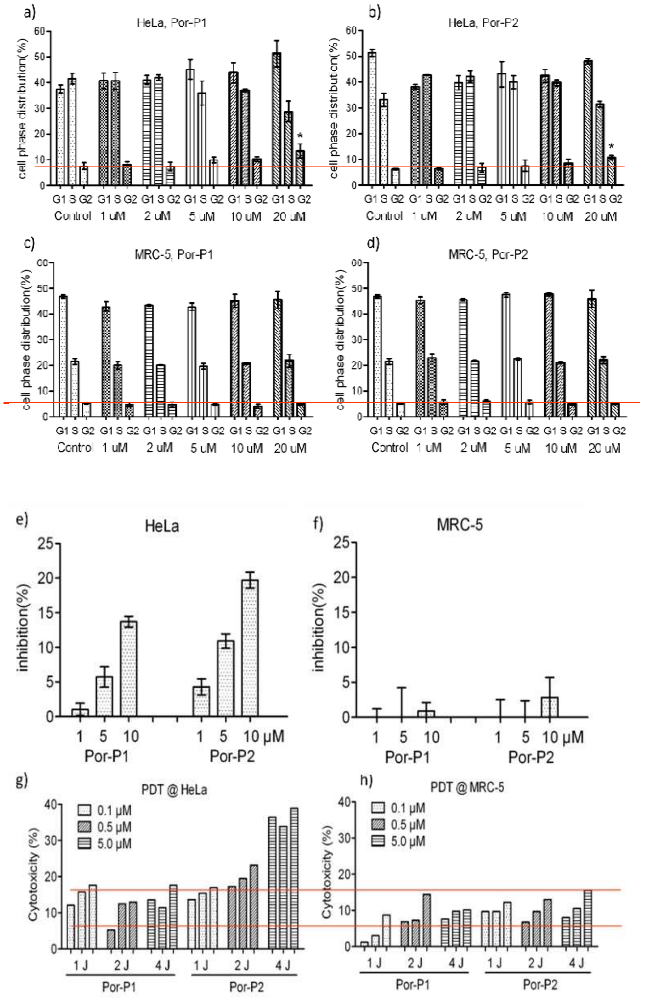

Fig. 3 (a)–(d) Cell cycle and (e)–(h) cell death studies (e-f, dark and g-h light cytotoxicity-the three columns of Y axis represent three concentrations of each dose of irradiation, 1 J , 2 J, and 4 J, of Por-**P1** and Por-**P2**.) of the Por-**P1** and Por-**P2**-treated cancer (HeLa) and normal (MRC-5) cell lines.

Cell phase distributions were then determined (Fig. 3a-d). Given that uncontrolled proliferation is the main feature of the cancer cell, it is possible to arrest the cancer growth by disrupting any phase of the cell cycle (G1, S, G2 and M). Added to this, it would be better if the agent can specifically function in cancer cells but not normal proliferating cells (such as liver, hematopoietic or germ cell) for safety concerns. Plk1 is a serine/threonine kinase that is essential for cell cycle mitotic progression, containing a unique PBD which can be selectively bound by phospho-mimic peptides or other analogs. Por-**P1** and Por-**P2** treated cancer cells show an increase in G2 phases ($P<0.01$), which indicates the potential of Plk1 inhibition. On the contrary, Por-**P1** and Por-**P2** show no effect on normal cells (the red line in Fig. 3c-d). Especially, Por-**P2** which has the ability to interrupt the cell cycle, where the cell phase distribution are ~50% (G1), ~30% (S) and ~12%(G2) phase after the cells dosed with Por-**P1**/Por-**P2**. But in the control, the phase distribution of cell division is ~52% (G1), ~34% (S) and ~6% (G2) respectively. (Fig. 3a and b)

As a potential anti-tumor agent, the selectivity toxicity parameter in the cancer/normal cell is of paramount importance. Both the Por-**P1** and Por-**P2** show the selectivity and dark cytotoxicity toward cancer cells. In effect, Por-**P2** exerts more significant inhibition effects (10% more) on HeLa cells than Por-**P1** under the same dosed concentration (Fig. 3e). The IC_{50} values of Por-**P1** and Por-**P2** in HeLa cells are 30 and 18 μM, respectively. In the normal MRC-5 cells, no significant inhibition effects are observed under the same experimental conditions (Fig. 3f). The IC_{50} in cancer cells is 10-fold less than in normal cells. (IC_{50} = Por-**P1** and Por-**P2** is ~0.5 μM) Plk1 inhibition causes cancer cell to undergo apoptosis, whereas exerts a slight effect on normal cell. In our work, porphyrin-Plk1 specific peptide conjugates (Por-**P1** and **P2**) possess dual functions of targeting and imaging of Plk1 in live cell as well as generating single oxygen to kill the target cells. Porphyrin moieties are well-known for producing reactive oxygen species upon photo-excitation and can be the new generation of "smart-cancer specific" photodynamic therapy agents via Plk1 binding *in vitro*. The photocytotoxicty of Por-**P1** and Por-**P2** was examined in the cancer and normal cell lines (Fig. 3g and 3h). Correlated results in the cancer/normal selectivity are observed in dark and light cytotoxicity for Por-**P1** and Por-**P2**. Significant cell deaths are only found in HeLa cells, but not in normal MRC-5 cells with the incubation of Por-**P1** and Por-**P2** under the same experimental conditions. Por-**P1** and Por-**P2** exhibit very similar singlet oxygen quantum yield. (~45% in CH_2Cl_2); the selectivity binding toward Plk1 can be the more critical factor for the greater light cytotoxicity in cancer cells. Fig. 3g and 3h show that Por-**P2** would be a better cancer-cell selective photodynamic therapy agent than Por-**P1**. Only a light dose of 4 J and 5 μM of Por-**P2** can ~40% cell deaths vastly be triggered in cancer cells. In contrast, in normal cells, the cytotoxicity is only ~15%. For Por-**P1**, under the same conditions, the cell deaths of HeLa cancer and normal MRC-5 cells were found to be only ~18% and ~12%, respectively.

Conclusions

In conclusion, we had synthesized a practical dual imaging and inhibition agent (Por-**P2**) for one of the most important kinase drug targets – Plk1. With a porphyrin moiety conjugated to a tailor-made Plk1 specific peptide we have prepared dual acting probes (Por-1 and Por-2) that show selective and responsive NIR emission with Plk1 in aqueous and *in vitro*. Por-2 also displays interruption of the cancer cell cycle and low IC_{50} values in cancer cells, but not in normal cells. Por-**P2** can, therefore, enable both Plk1 imaging and cancer cell division inhibition. This dual mode of action means that systems like Por-2 are apromising class of molecules for the further development of new anti-cancer agents.

Experimental Section

General information for syntheses. All the chemicals were purchased commercially and used without further purification. All analytical grade solvents were dried by standard procedures. Merck silica gel (60, particle size 0.040-0.063 mm) was used for flash column chromatography. NMR spectra were recorded on Brüker Advance 400 (^{1}H: 400 MHz, ^{13}C: 100 MHz). The following abbreviations were used to explain the multiplicities: s = singlet, d = doublet, t = triplet, q = quartet, m = multiplet, br = broad. High resolution mass spectra were obtained from Applied Biosystems (ABI) Q-Star Elite MALDI-TOF mass spectrometer. Electrospray ionization mass spectra (ESI-MS) were acquired on a Finnigan MAT LCQ mass spectrometer. The synthetic routes for all compounds were described in the figure S1 in the ESI†. The compound Zn-Por-1-H were prepared by the methods we published previously.[15]

Synthesis of Plk1 specific peptides (P1 and P2). The two peptides were obtained by a stepwise elongation of the peptide chain by the method outlined below: 0.5 g of the rink amide resin (0.45 mmol/g loading) was suspended in a 20% solution of piperidine in DMF, stirred for 20 min at room temperature, and washed with DMF prior to use in subsequent steps. The first amino acid to be coupled, Fmoc-(Bn-p)-Thr-OH (420 mg, 4 equiv) for P1 (Fmoc-(tBu)-Asp-OH for P2) was dissolved in DMF and then coupled to the resin in the presence of PyBOP (645 mg, 4 equiv) and NMM (135 μl, 4 equiv) with the use of microwave chemistry as described previously.[12] Other Fmoc amino acid derivatives: Fmoc-Ser(^{t}Bu)-OH (420 mg, 4 equiv), Fmoc-His(Trt)-OH (438 mg, 4 equiv), Fmoc-Leu-OH (350 mg, 4 equiv), Fmoc-Pro-OH (320 mg, 4 equiv) were connected to the resin using an analogous synthetic strategy. Following the final removal of the Nα-Fmoc group, the peptide-resin was washed with DMF. The free peptide was obtained by cleavage through the use of 9 ml of TFA in the presence of 750 μl of water and 750 μl of TIPS according to the standard procedure.[12] Following the cleavage, the peptide was purified by using preparative HPLC. The main peptide-containing fractions were collected and lyophilized. The purity of peptides were confirmed by HPLC. **P1**: PLHSpT ESI-MS (m/z): Calcd for $C_{24}H_{41}N_8O_{10}P$, 632.2683; found for $[M+H]^+$, 633.2584; **P2**: PLHSD ESI-MS (m/z): Calcd for $C_{24}H_{37}N_7O_9$, 567.2653; found for $[M+H]^+$, 568.2396.

Synthesis of Por-NH_2. Zn-Por-1-H [15] (200mg) was dissolved in 5ml of dry THF, and added to the solution of 4-iodoaniline (10 equiv.) in 10ml of THF followed by $Pd(PPh_3)_2Cl_2$ (2omg) and CuI (12mg) at 50 °C. After that, 3 ml of triethylamine was added. The resulting solution was stirred for 12 h at the same temperature. The solid catalysts were filtered out and the solution was concentrated. The residue was purified via a silica gel column. Purple solid, as the intermediate, was collected and characterized. ^{1}H NMR ($CDCl_3$) δ, 3.95 (s, 18H), 4.17 (s, 9H),7.45 (m, 7H), 7.64 (m, 4H), 7.90 (d, J = 4 Hz, 2H) 8.22 (d, J = 4 Hz, 2H), 8.88 (d, J = 2 Hz, 2H,) 8.90, (d, J = 2 Hz, 2H) HRMS (m/z): Calcd for $C_{61}H_{51}N_5O_9Zn$, 1061.2978; found for $[M+1]^+$, 1061.2950. When the intermediate was dissolved in 5 ml of THF, 5ml of 10% HCl was also added for subsequent stirring for 2h at room temperature. The stirred solution was then neutralized with 1M NaOH and extracted with CH_2Cl_2. The organic phase was dried with anhydrous Na_2SO_4, and further concentrated, with the residue being purified on a short silica gel column. Purple solid, Por-NH_2, as the title product was collected. ^{1}H NMR ($CDCl_3$): δ, -2.80 (s, 2H), 3.94 (s, 18H), 4.14 (s, 9H),7.46 (m, 7H), 7.62 (m, 4H), 7.90 (d, J = 4 Hz, 2H) 8.18 (d, J = 4 Hz, 2H), 8.87 (d, J = 2 Hz, 2H,) 8.98, (d, J = 2 Hz, 2H); ^{13}C NMR ($CDCl_3$): δ, 87.1, 91.5, 106.2, 107.5, 107.8, 112.2, 112.7, 114.6, 119.6, 120.0, 123.4, 129.6, 131.1, 132.9, 134.4, 137.5, 137.7, 141.3, 146.8, 151.3; HRMS (m/z): Calcd for $C_{61}H_{53}N_5O_9$, 999.3843; found for $[M+H]^+$, 1000.3625.

Synthesis of Por-COOH. Dihydro-2H-pyran-2,6(3H)-dione(34mg, 0.30mmol) was first added into the solution of Por-NH_2 (100mg, 0.10mmol) in DCM. The resulting solution was stirred for 6h at room temperature, giving the titled purple solid product after purification (102mg, 0.092mmol, 92%). ^{1}H NMR($CDCl_3$) δ, -2.80 (s, 2H), 2.10-2.13 (m, 6H), 2.51-2.55 (m, 4H), 3.97 (s, 18H), 4.18 (s, 9H), 7.50 (s, 8H), 7.60-7.66 (m, 4H), 7.92 (d, J = 4Hz, 2H) 8.20 (d, J = 4Hz, 2H), 8.88 (d, J = 2Hz, 2H), 8.98, (m, 6H); ^{13}C NMR ($CDCl_3$): δ, 20.6, 32.9, 36.3, 56.4, 61.3, 89.0, 90.5, 112.8, 118.9, 119.5, 119.6, 120.1, 122.9, 129.9, 131.0, 132.6, 134.5, 137.5, 137.9, 138.1, 142.0, 151.4, 170.8, 176.7; HRMS (m/z): Calcd for $C_{60}H_{60}N_5O_{12}$, 1113.4160; found for $[M+H]^+$, 1114.4279.

Synthesis of Por-P1 and Por-P2. A stirred solution of the acid Por-COOH (0.05 mmol) in anhydrous DMF (2 mL) was mixed with benzotriazol-1-yl-oxytripyrrolidinophosphonium hexafluorophosphate (PyBop) (0.15mmol), N,N-diisopropylethylamine (DIPEA) (0.30 mmol). After 10 minutes stirring at room temperature for the activation of carboxylate, this solution was added over the resin-bounded peptides (**P1**/**P2**) (0.017 mmol). Nitrogen gas was passed through the resin suspension for 8 h. The resin was then filtered and washed with DMF (3mL × 3 × 3min). General procedures for global deprotection and cleavage from the resin are listed: A 2 mL of cleavage cocktail (150 μL of CH_2Cl_2, 75 μL of TIS, and TFA to 2mL) was added to the resin-bounded coupling products. The resulting mixture was passed with N_2 and mixed for 8 hours. The resin was then filtered, and the TFA filtrate was concentrated under reduced pressure. The residue was washed with diethyl ether and dried under reduced pressure to afford the products as purple solids, Por-P1 HRMS (m/z): Calcd for $C_{90}H_{98}N_{13}O_{21}P$, 1727.6738; found for $[M+H]^+$, 1728.6824; Por-P2 HRMS (m/z): Calcd for $C_{90}H_{93}N_{13}O_{19}$, 1661.6867; found for $[M+H]^+$, 1662.6970.

Photo-physical Measurement. UV-Visible absorption spectra in the spectral range 200 to 1100 nm were recorded by an HP Agilent UV-8453 Spectrophotometer. Single-photon luminescence spectra were recorded using an Edinburgh instrument FLS920 combined fluorescence lifetime and steady state spectrophotometer that was equipped with a visible to near-infrared-sensitive photomultiplier in nitrogen flow cooled housing. The spectra were corrected for detector response and stray background light phosphorescence. The quantum yields of the compounds were measured by the comparative method and integrated sphere.[14] Singlet oxygen was detected directly by its phosphorescence emission at 1270 nm using an InGaAs detector on a PTI QM4 luminescence spectrometer. The singlet oxygen quantum yields (Φ_Δ) of the test compounds were determined in $CHCl_3$ by comparing the singlet oxygen emission intensity of the sample solution to that of a reference compound (H_2TPP, $\Phi_\Delta = 0.55$ in $CHCl_3$).[15]

Stability Test via Titration. Titration experiments were conducted to investigate the effect of several common biological cations and HSA on the two porphyrin moieties. Liquid concentrated stock solutions of each anion, as well as HSA, were added individually and gradually to a solution of the compound concerned. Addition was ceased either when the volume of added anion totaled 5% of the compound solution or the influence on compound luminescence was saturated. Single-photon luminescence spectra were determined via the aforementioned procedures.

Molecular Modelling. Molecular docking calculation of Plk1 specific peptides and their porphyrin-pepides complexes (Por-**Pn**) were performed using AutoDock Vina software which was released by Dr. Oleg Trott in the Molecular Graphics Lab at The Scripps Research Institute.[15] Crystal structure of Plk1 protein (PDB code: 3RQ7) were transformed to PBDQT document in AutoDocTools-1.5.4 to set the docking surface (center_x = 1.34; center_y = 20.166; center_z = 27.784; and size_x = 44; size_y = 30; size_z = 6). Peptides and their Por-**Pn** complexes were graphed by GaussView and then subjected to torsions setting in AutoDocTools-1.5.4, to be saved as pdbqt files.[15] Binding conformations and affinities were processed in DOS (window XP). Results were presented as the best binding types and affinity values (kCal/mol).

Cell Culture. Human cervical cancer HeLa cells were grown in Dulbecco's Modified Eagle Medium (DMEM) supplemented with 10 % fetal bovine serum (FBS) 1 % penicillin and streptomycin at 37 ^oC and 5 % CO_2. Human lung diploid fibroblasts MRC-5 were provided by Cell resource center of Shanghai Institute of Biological Sciences, Chinese Academy of Sciences; and cultured in MEM (GIBCO 41500034) supplemented with 10 fetal bovine serum, 1% penicillin and streptomycin at 37 ^oC and 5 % CO_2.

MTT Cell Cytotoxicity Assay. HeLa or MRC-5 cells treated with Por-**P1**/Por-**P2** for 24 hours were further incubated with MTT, 3-(4, 5-dimethylthiazol-2-yl)-2 and 5-diphenyltetrazolium bromide (0.5 mg/ml) for 4 h. Formazans were produced during cell metabolism .which were to be thoroughly dissolved by dimethyl sulfoxide (DMSO). The absorbances of solutions were measured in Bio-Rad iMark microplate reader (490 nm) and quadruplicates were performed. Data analysis and plotting were operated by the GraphPad Prism 5 software.

Antibodies and Western blotting. Anti Plk1 and anti-Rb (p-807) antibodies were purchased from Santa Cruz Biotechnology (sc-17783). Anti-cyclin A, cyclin B1, tubulin, CDK1, CDK2 and Geminin antibodies were used as described in Lab. HeLa cells seeded in 12 well-plate were treated with Por-**P1** or Por-**P2** (1, 10, 20 μM each) for 24 h, and the cells were washed in PBS twice after removal of the culture medium. Directly lysis in 50 mM Tris-HCl, pH=6.8, 1% SDS, 5% glycerol was employed and they were thoroughly denatured in boiling water bath. After centrifugations, the supernatant was collected as clear lysis. An equal amount of cell proteins were loaded onto the 10% SDS-PAGE gel to allow electrophoresis separation. Finally, proteins were transferred into nitrocellular membranes from the gel and followed by western blotting process. The proteins were probed by antibodies, accordingly and respectively. The final graphs were developed using the chemiluminescence procedure (ECL, Pierce).

Flow Cytometry. 106 cells were harvested by trypsin digestion and washed twice in PBS, and then fixed in 70% ethanol for 2 h at 4 ^oC. After removal of ethanol, cells were resuspended in PBS and then subjected to PI staining (1% triton X-100, 50 μg/ml RNase A, 20 μg/ml propidium iodide) for 40 min, at 37 ^oC. Cell phase distributions were analyzed in BD FACSCalibur and the results were processed by FlowJo 7.6.1, illustrated as Half-Offset histogram and column charts (for calculation of cell phases distributions).

Confocal In Vitro Imaging. Cells were seeded on coverslip in 35-mm culture dishes overnight. The cells were initially incubated with the compounds (1 μM). Then the unabsorbed chemicals were washed away with PBS and the cells were subject to confocal microscopic imaging. All images were captured using the Leica SP5 (upright configuration) confocal microscope inside the tissue culture chamber (5% CO_2, 37 ^oC). The excitation beam produced by the Argon laser/LED, which was tunable from 432 nm, 457 nm, 476 nm, 488 nm, 514 nm and 800 nm to 1000 nm (fs laser) and focused on the adherent cells through a 40x/60x oil immersion objective.

Acknowledgements

This work was funded by grants from The Hong Kong Research Grants Council (HKBU 203013), ESPRC, Durham University, Hong Kong Baptist University (FRG 2/12-13/002).

Notes and references

[a] Department of Chemistry, Hong Kong Baptist University, Kowloon Tong, Hong Kong SAR; Email: klwong@hkbu.edu.hk
[b] Department of Chemistry, Durham University, Durham, DH1 3LE, UK; Email: s.l.cobb@durham.ac.uk
[c] Department of Biology, Hong Kong Baptist University, Kowloon Tong, Hong Kong SAR;
[d] Department of Biology and Chemistry, City University of Hong Kong, Kowloon Tong, Hong Kong SAR;
[e] Hong Kong Baptist University Institute of Research and Continuing Education, Shenzhen, P. R. China. Email: rongfengl@hkbu.edu.hk
Electronic Supplementary Information (ESI) available: High resolution mass spectra of P1 and P2; NMR spectra of lig-ands of Por-**P1** and Por-**P2**; Synthetic Routes; Absorption and emission spectra of Por-**P1** and Por-**P2**. Raw data of flow cytometry. See DOI: 10.1039/b000000x/

1. S. M. Kim, S. Yoon, N. Choi, K. S. Hong, R. N. Murugan, G. Cho and E. K. Ryu, *Biomaterials*, 2012, **33**, 6915-6225.
2. D. M. Glover, I. M. Hagan and Á. A. M. Tavares, *Gene. Dev.*, 1998, **12**, 3777-3787.
3. M. E. Burkard, A. Santamaria and P. V. Jallepalli, *ACS Chem. Bio.*, 2012, **7**, 978-981.
4. A. K. L. Cheung, J. C. K. Ip, H. L. Lung, J. Z. Wu, S. W. Tsao and M. L. Lung, *Mol. Cancer Ther.*, 2013, **12**, 1393-1401.
5. M. Steegmaier, M. Hoffmann, A. Baum, P. Lenart, M. Petronczki, M. G. Krssak, U., P. L. Garin-Chesa, S., J. Quant, M. Grauert, G. R. Adolf, N. Kraut and J.-M. a. R. Peters, W., *Curr. Bio.*, 2007, **17**, 316-322.
6. C. V. Miduturu, X. Deng, N. Kwiatkowski, W. Yang, L. Brault, P. Filippakopoulos, E. Chung, Q. Yang, J. Schwaller, S. Knapp, R. W. King, J.-D. Lee, S. Herrgard, P. Zarrinkar and N. S. Gray, *Chem.Biol.*, 2011, **18**, 868-879.
7. M. E. Burkard, J. Maciejowski, V. Rodriguez-Bravo, M. Repka, D. M. Lowery, K. R. Clauser, C. Zhang, K. M. Shokat, S. A. Carr, M. B. Yaffe and P. V. Jallepalli, *PLoS Biol.*, 2009, **7**, e1000111.
8. I. Beria, D. Ballinari, J. A. Bertrand, D. Borghi, R. T. Bossi, M. G. Brasca, P. Cappella, M. Caruso, W. Ceccarelli, A. Ciavolella, C. Cristiani, V. Croci, A. De Ponti, G. Fachin, R. D. Ferguson, J. Lansen, J. K. Moll, E. Pesenti, H. Posteri, R. Perego, M. Rocchetti, P. Storici, D. Volpi and B. Valsasina, *J. Med. Chem.*, 2010, **53**, 3532-3551.
9. M. O. Duffey, T. J. Vos, R. Adams, J. Alley, J. Anthony, C. Barrett, I. Bharathan, D. Bowman, N. J. Bump, R. Chau, C. Cullis, D. L. Driscoll, A. Elder, N. Forsyth, J. Frazer, J. Guo, L. Guo, M. L. Hyer, D. Janowick, B. Kulkarni, S.-J. Lai, K. Lasky, G. Li, J. Li, D. Liao, J. Little, B. Peng, M. G. Qian, D. J. Reynolds, M. Rezaei, M. P. Scott, T. B. Sells, V. Shinde, Q. J. Shi, M. D. Sintchak, F. Soucy, K. T. Sprott, S. G. Stroud, M. Nestor, I. Visiers, G. Weatherhead, Y. Ye and N. D' Amore, *J. Med. Chem.*, 2012, **55**, 197-208.
10. F. Liu, J.-E. Park, W.-J. Qian, D. Lim, A. Scharow, T. Berg, M. B. Yaffe, K. S. Lee and T. R. J. Burke, *ACS Chem. Bio.*, 2012, **7**, 805-810.
11. P. Lenart, M. Petronczki, M. Steegmaier, B. Di Fiore, J. J. Lipp, M. Hoffmann, W. J. Rettig, N. Kraut and J. M. Peters, *Curr. Bio.*, 2007, **17**, 304-315.
12. J. Liu, W. D. Gray, M. E. Davis and Y. Luo, *Interface Focus*, 2012, **2**, 307-324.
13. O. Trott and A. J. Olson, *J. Comput. Chem.*, 2010, **31**, 455-461.
14. Y. Li, T. M. Pritchett, J. Huang, M. Ke, P. Shao and W. Sun, *J. Phys. Chem. A.*, 2008, **12**, 7200-7207.
15. J. Zhang, C.-F. Chan, J.-W. Zhou, T. C.-K. Lau, D. W. J. Kwong, H.-L. Tam, N. K. Mak, K.-L. Wong and W. K. Wong, *Bioconjugate Chem.*, 2012, **23**, 1623-1638.

